Molecular Cell
Article

Mutations in the Intellectual Disability Gene *Ube2a* Cause Neuronal Dysfunction and Impair Parkin-Dependent Mitophagy

Dominik M. Haddad,[1,2] Sven Vilain,[1,2] Melissa Vos,[1,2] Giovanni Esposito,[1,2] Samer Matta,[1,2] Vera M. Kalscheuer,[3] Katleen Craessaerts,[1,2] Maarten Leyssen,[1,2] Rafaella M.P. Nascimento,[4] Angela M. Vianna-Morgante,[4] Bart De Strooper,[1,2] Hilde Van Esch,[2] Vanessa A. Morais,[1,2,*] and Patrik Verstreken[1,2,*]
[1]VIB Center for the Biology of Disease, 3000 Leuven, Belgium
[2]KU Leuven, Center for Human Genetics and Leuven Research Institute for Neuroscience and Disease (LIND), 3000 Leuven, Belgium
[3]Max Planck Institute for Molecular Genetics, Department of Human Molecular Genetics, Ihnestrasse 73, 14195 Berlin, Germany
[4]Department of Genetics and Evolutionary Biology, Institute of Biosciences, University of São Paulo, São Paulo, 05508-060 Brazil
*Correspondence: vanessa.morais@cme.vib-kuleuven.be (V.A.M.), patrik.verstreken@cme.vib-kuleuven.be (P.V.)
http://dx.doi.org/10.1016/j.molcel.2013.04.012

SUMMARY

The prevalence of intellectual disability is around 3%; however, the etiology of the disease remains unclear in most cases. We identified a series of patients with X-linked intellectual disability presenting mutations in the *Rad6a* (*Ube2a*) gene, which encodes for an E2 ubiquitin-conjugating enzyme. *Drosophila* deficient for *dRad6* display defective synaptic function as a consequence of mitochondrial failure. Similarly, mouse *mRad6a* (*Ube2a*) knockout and patient-derived *hRad6a* (*Ube2a*) mutant cells show defective mitochondria. Using in vitro and in vivo ubiquitination assays, we show that RAD6A acts as an E2 ubiquitin-conjugating enzyme that, in combination with an E3 ubiquitin ligase such as Parkin, ubiquitinates mitochondrial proteins to facilitate the clearance of dysfunctional mitochondria in cells. Hence, we identify RAD6A as a regulator of Parkin-dependent mitophagy and establish a critical role for RAD6A in maintaining neuronal function.

INTRODUCTION

Intellectual disability (ID) represents a significant social and economic burden. About 3% of the Western population is diagnosed with ID, and patients require lifelong care (Backx et al., 2010). Numerous genetic causes of ID exist, in particular X-linked ID (XLID); however, assessment of the molecular defects that result in synaptic deficits as well as prognostication for therapeutic care remain a challenge (Baker et al., 2012).

Mutations in *hRad6a* (*Ube2a*) cause XLID, but how this gene affects neuronal function is not known (Budny et al., 2010; de Leeuw et al., 2010; Honda et al., 2010; Nascimento et al., 2006). RAD6A is a neuronally expressed ubiquitin conjugating enzyme (E2) (Jentsch et al., 1987; Koken et al., 1996). RAD6-dependent ubiquitination is best studied in DNA damage tolerance (Karras and Jentsch, 2010; Koken et al., 1996, 1991; Prakash, 1994), a process that allows specialized DNA polymerases to bypass DNA lesions (Lee and Myung, 2008). Several nuclear E3 ubiquitin ligases that act with RAD6 have been identified, including *Rad18*, *Ubr1*, and *Bre1* (Game and Chernikova, 2009). Although RAD6A is rather well studied in the nucleus, it remains unclear how mutant RAD6A translates into dysfunction of the nervous system. Moreover, RAD6A is abundantly present in the cytoplasm (Zenkel et al., 2007), and the non-nuclear roles for RAD6A need further exploration.

We find that RAD6A is an E2 ubiquitin-conjugating enzyme that, in combination with an E3 ubiquitin ligase such as Parkin (Martin et al., 2011), controls clearance of dysfunctional mitochondria in mice and in human cells in vitro. Our work identifies RAD6A as a ubiquitin-conjugating enzyme (E2) essential to maintain a healthy mitochondrial pool in vivo; this is critical to maintain normal synaptic transmission and potentially an important element involved in the etiology of ID.

RESULTS

Identification of *Rad6a* Mutations in XLID Patients

To identify the causative gene defect in 248 unresolved XLID families, we performed X-exome sequencing. This strategy allowed us to identify two families that carry a pathogenic mutation in *hRad6a* (*Ube2a*) (Figure 1A and Table S1). Mutations in *hRad6a* were recently linked to XLID using a positional candidate gene approach (Budny et al., 2010; Nascimento et al., 2006). We found a frameshift mutation leading to a deletion, I87MfsX14 (X:118600597-98 TA deletion), and a missense mutation, R7W (X:118592721 C→T), affecting a highly conserved amino acid in exon 1 of *hRad6a* in affected males and their carrier mothers from families a and b, respectively. These mutations were not identified in 389 control samples. All affected males of these two families display ID as well as other developmental features (Table S1 and Supplemental Experimental Procedures); however, the underlying mechanisms that result in neuronal defects remain elusive.

Next we determined if the mutations in *hRad6a* affect expression of RNA or protein. Mammals harbor *Rad6a* and *Rad6b* proteins that are 80% identical at the sequence level. To assess

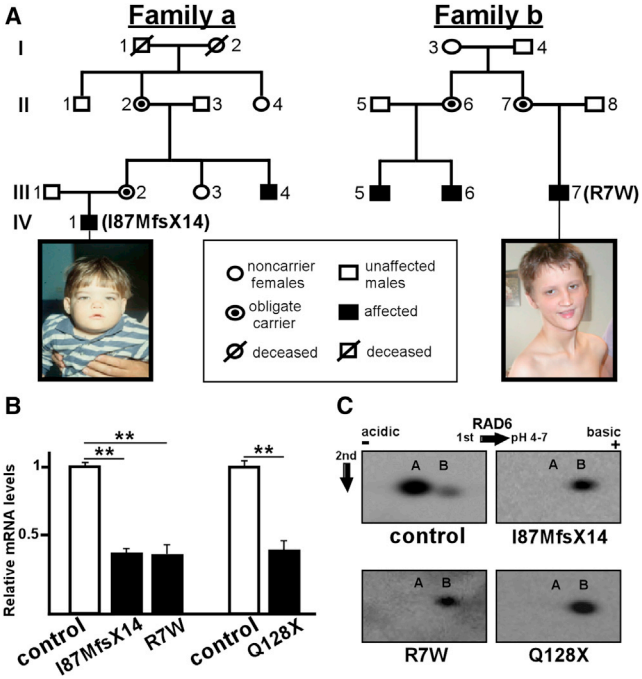

Figure 1. *Rad6a* Mutations in XLID Patients

(A) Pedigrees of families a and b, showing affected males I87MfsX14 (a-IV.1) and R7W (b-III.7) and carrier females (related to Table S1). *Rad6a* was also identified in an independent screen for defects in synaptic and mitochondrial dysfunction (Figure S1).

(B) *hRad6a* mRNA levels in I87MfsX14 and R7W lymphocytes and Q128X fibroblasts. Data are mean ± SEM for three experiments; ANOVA post hoc Dunnett's test: $^{**}p < 0.01$.

(C) IEF/SDS-PAGE using whole-cell extract from I87MfsX14 and R7W lymphocytes and from Q128X fibroblasts probed with anti-RAD6. The first dimension is isoelectrical focusing with a pH gradient of 4–7, and the second dimension is an SDS-PAGE. "A" and "B" denote hRAD6A and hRAD6B protein spots (two independent experiments). Longer exposures also did not reveal hRAD6A signal (not shown).

hRAD6A expression in lymphocytes from patients, as well as in fibroblasts from a previously reported Brazilian patient harboring a frameshift mutation, Q128X (c.382C→T) (Nascimento et al., 2006), we used RT-PCR and two-dimensional (2D) analysis (isoelectric focusing [IEF]/SDS-PAGE). While *hRad6a* messenger RNA (mRNA) levels are decreased by approximately 60% in cells harboring the clinical mutations (Figure 1B), hRAD6A protein is not detected. However, the closely related hRAD6B is expressed (Figure 1C). Thus, we identified two families in which mutations in the *hRad6a* gene cause XLID. Analysis of patient cells harboring these *hRad6a* mutations indicate the mutant RAD6A protein is not expressed or is below our detection limit.

RAD6A Is Required for Mitochondrial Function across Species

ID, at least in part, may originate from defects in synaptic transmission. Interestingly, in a *Drosophila* RNA interference (RNAi)-based screen for defects in synaptic and mitochondrial function, two processes linked to synaptic transmission (Chan, 2006), we identified *dRad6* (*UbcD6*) (Figure S1). Based on RNAi-mediated knockdown, loss of *dRad6* function results in locomotion defects, reduced synaptic vesicle trafficking, and mitochondrial dysfunction at neuromuscular junctions (NMJs) (Figure S1 and Table S2).

RAD6A has been studied mostly for its role in the nucleus, but the protein is also abundantly present in the cytoplasm. To verify if the synaptic phenotypes we observed upon *dRad6* RNAi in *Drosophila* are specific to the loss of *dRad6* function, we used a transposon insertion in *dRad6* ($dRad6^{EY}$) and created an imprecise excision of this P element ($dRad6^{\Delta 1}$). Both alleles result in reduced protein expression (Figures S2A and S2B) and cause second instar/early third instar lethality when homozygous. The lethality as well as all the phenotypes we report are rescued by a genomic $dRad6^{+}$ fragment, indicating that defects we observe are only associated with loss of *dRad6* function.

The early lethality of *dRad6* mutants precludes us from analyzing phenotypes in adults. However, we were able to measure the mitochondrial membrane potential ($\Delta\psi m$) at *dRad6* mutant NMJs using JC-1, a potentiometric green fluorescent dye that shifts to red fluorescence within mitochondria with a normal negative $\Delta\psi m$. In contrast to controls, we observe reduced red JC-1 labeling in mitochondria of $dRad6^{\Delta 1}$ and $dRad6^{EY}$ mutant NMJs (Figures 2A and 2B), very similar to labeling of synaptic mitochondria upon *dRad6* RNAi expression (Figure S1). This defect in JC-1 labeling in *dRad6* mutants is rescued by $dRad6^{+}$ (Figures 2A and 2B). Hence, mitochondria in *dRad6* mutant neurons display a defect to maintain their $\Delta\psi m$.

To determine if the mitochondrial defects in *dRad6* mutants are evolutionary conserved, we used knockout mouse embryonic fibroblasts (MEFs) (Figures 2C, 2D, and S2C) (Koken et al., 1996; Roest et al., 2004) and lymphocytes that express the hRAD6A R7W and I87MfsX14 clinical mutations (Figures 2E and 2F). We also used patient fibroblasts expressing hRAD6A Q128X (Figures 2G and 2H). To quantify alterations in $\Delta\psi m$, we assessed the fluorescence of tetramethyl rhodamine ethyl ester (TMRE), a dye that concentrates in polarized mitochondria (Figure S2D). In contrast to control cells, mitochondria in *mRad6a* null MEFs or in patient-derived cells show significantly less TMRE labeling (Figures 2C–2H). This defect is specific to the loss of *Rad6a* because expression of wild-type *mRad6a* in knockout cells rescues the defect (Figures 2C, 2D, and S2E). Thus, loss of mRAD6a and hRAD6A in mouse- and patient-derived cells, respectively, results in mitochondrial dysfunction.

Neuronal Dysfunction in *dRad6 Drosophila* Mutants

Vesicle mobilization and neurotransmission are ATP-dependent processes, and mitochondrial function is related to the regulation of neuronal communication (Morais et al., 2009; Stowers et al., 2002; Verstreken et al., 2005). In our RNAi screen we found that knockdown of *dRad6* results in reduced stimulation-dependent vesicle recycling as gauged by bouton labeling of FM1-43 (Figure S1). FM1-43 is a membrane-bound fluorescent dye that, upon neuronal stimulation, is internalized by newly forming synaptic vesicles (Verstreken et al., 2008). Similarly, NMJ boutons of $dRad6^{\Delta 1}$ and $dRad6^{EY}$ mutants also display less FM1-43 labeling upon stimulation when compared to controls, and this defect is rescued by $dRad6^{+}$ (Figures 3A and 3B). The data indicate defects in synaptic vesicle trafficking in *dRad6* mutants.

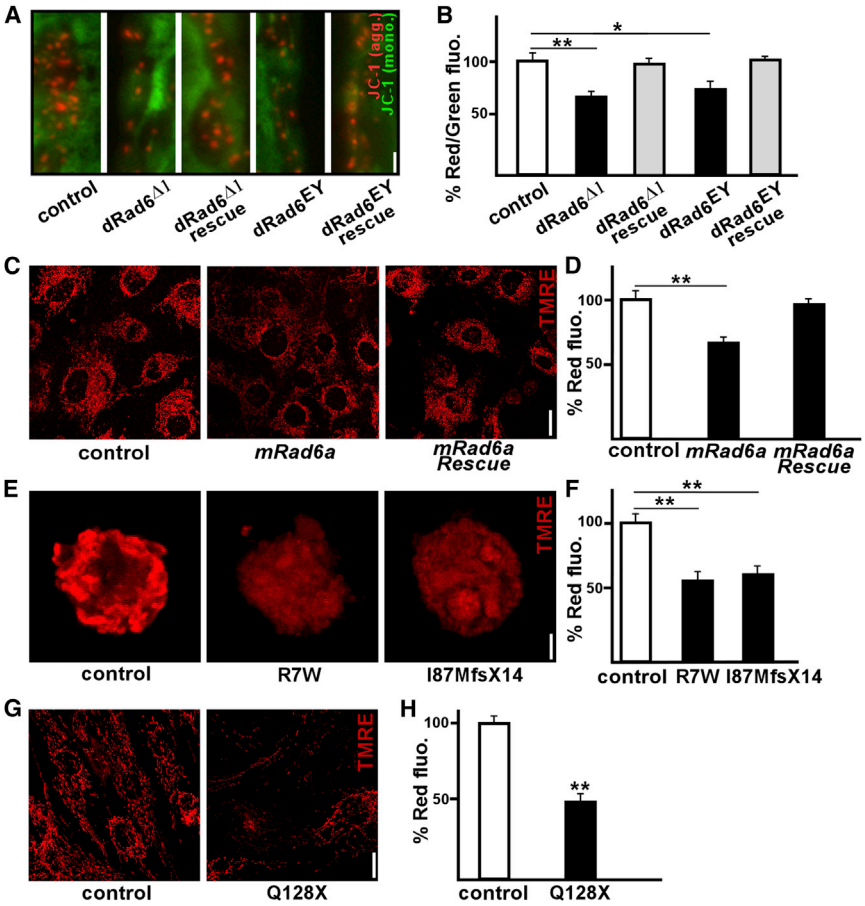

Figure 2. Mitochondrial Defects in *Rad6* Mutant Fly, Mouse, and Human Cells

(A and B) Imaging of $\Delta\psi$m at third instar larval boutons of controls, mutants *dRad6*$^{\Delta 1}$ and *dRad6*^{EY}, and mutants that express wild-type dRAD6, using JC-1 (red, JC-1 aggregates; green, JC-1 monomers; scale bar = 4.5 μm) (A), and quantification of red over green fluorescence in synaptic mitochondria normalized to control (B). RAD6 expression levels are shown in Figures S2A and S2B. Data are mean ± SEM, n = 6; ANOVA post hoc Dunnett's test: *p < 0.05, **p < 0.01.

(C and D) Control and *mRad6a* null MEFs and *mRad6a* null MEFs expressing wild-type mRAD6A labeled with tetramethylrhodamine ethyl ester (TMRE) to assess $\Delta\psi$m (C) (scale bar = 40 μm) and quantification of TMRE fluorescence in mitochondria normalized to control (D). Expression levels of mRAD6A, mRAD6B, and mRAD6A-Myc shown in Figures S2C and S2E. TMRE fluorescence in FCCP-treated cells shown in Figure S2D. Data are mean ± SEM, n = 50 cells from three experiments; ANOVA post hoc Dunnett's test: **p < 0.01.

(E and F) Control and patient-derived *hRad6a* mutants I87MfsX14 and R7W lymphocytes labeled with TMRE (E) to assess $\Delta\psi$m (scale bar for [E] = 5 μm) and corresponding quantification of TMRE fluorescence in mitochondria normalized to control (F). Data are mean ± SEM; n = 20 cells from two experiments; ANOVA post hoc Dunnett's test: **p < 0.01.

(G and H) Control and patient-derived *hRad6a* mutant Q128X fibroblasts labeled with TMRE (G) to assess $\Delta\psi$m (scale bar for [G] = 40 μm) and corresponding quantification of TMRE fluorescence in mitochondria normalized to control (H). Data are mean ± SEM; n = 20 cells from two experiments; t test: **p < 0.01.

To further test if the synaptic defects in *dRad6* mutants result in neurotransmission defects, we performed electrophysiology at the larval NMJ. First, we recorded excitatory junctional currents (EJCs) using a two-electrode voltage clamp (TEVC) by electrically stimulating the motor neuron and assessing the postsynaptic response. We did not observe a difference in EJC amplitude when recording in hemolymph-like saline solution (HL-3) with 0.5 mM external calcium (Figures 3C and 3D). Likewise, the average mEJC amplitude elicited by spontaneous vesicle fusions recorded in HL-3 with 0.5 mM $CaCl_2$ and tetrodotoxin is similar in controls and mutants (Figure 3E) as well as the quantal content (EJC/mEJC) (Figure 3F). Hence, under these conditions, synaptic transmission is not affected.

Reduced FM1-43 dye uptake is often the result of defects in synaptic vesicle recycling. We therefore recorded excitatory junctional potentials (EJPs) in HL-3 with more calcium (2 mM) during prolonged stimulation at different frequencies (1–20 Hz), as such conditions stimulate synaptic vesicle recycling (Dickman et al., 2005). At low-frequency stimulation (1 Hz) *dRad6* mutants maintain release (Figure 3G), but at higher frequencies (7–20 Hz) they fail to maintain transmission at the same level as controls (Figure 3H). When stimulated for 10 min at 10 Hz, the EJP amplitudes in *dRad6* mutants runs down (*dRad6*^{EY}: 66.2% ± 5.4%; *dRad6*$^{\Delta 1}$: 67.2% ± 3.5%). In controls or in *dRad6* mutants that harbor *dRad6*$^{+}$, EJPs are well maintained (control: 93.0% ± 8.9%; *dRad6*^{EY}; *dRad6*$^{+}$: 90.9% ± 1.5%; *dRad6*$^{\Delta 1}$; *dRad6*$^{+}$: 95.4% ± 2.7%; $p < 0.01$) (Figures 3I–3K). Thus, loss of dRAD6 function results in a reduced rate of vesicle replenishment at synapses.

To assess if the defect in neuronal communication in *dRad6* mutants is linked to mitochondrial dysfunction in *dRad6* mutants, we forward filled motor neurons with 1 mM ATP (Verstreken et al., 2005) and tested their ability to maintain neurotransmitter release during 10 Hz stimulation. Compared to mutants not incubated in ATP, EJPs recorded from mutant animals in which motor neurons were filled with ATP did not run down as much (*dRad6*^{EY} + ATP: 87.4% ± 8.7%; *dRad6*$^{\Delta 1}$ + ATP: 86.6% ± 4.1%; $p < 0.01$) (Figures 3I–3K). These data are consistent with the idea that the defects in neuronal communication are the result of reduced ATP as a consequence of mitochondrial dysfunction in *dRad6* mutants.

RAD6A Facilitates CCCP-Induced Mitochondrial Ubiquitination and Autophagy

We show that loss of RAD6A results in a pool of defective mitochondria in fly, mouse, and human cells. This deficit could be due in part to an impairment in defective mitochondria clearance by mitophagy (Narendra et al., 2009). Given that mitophagy requires

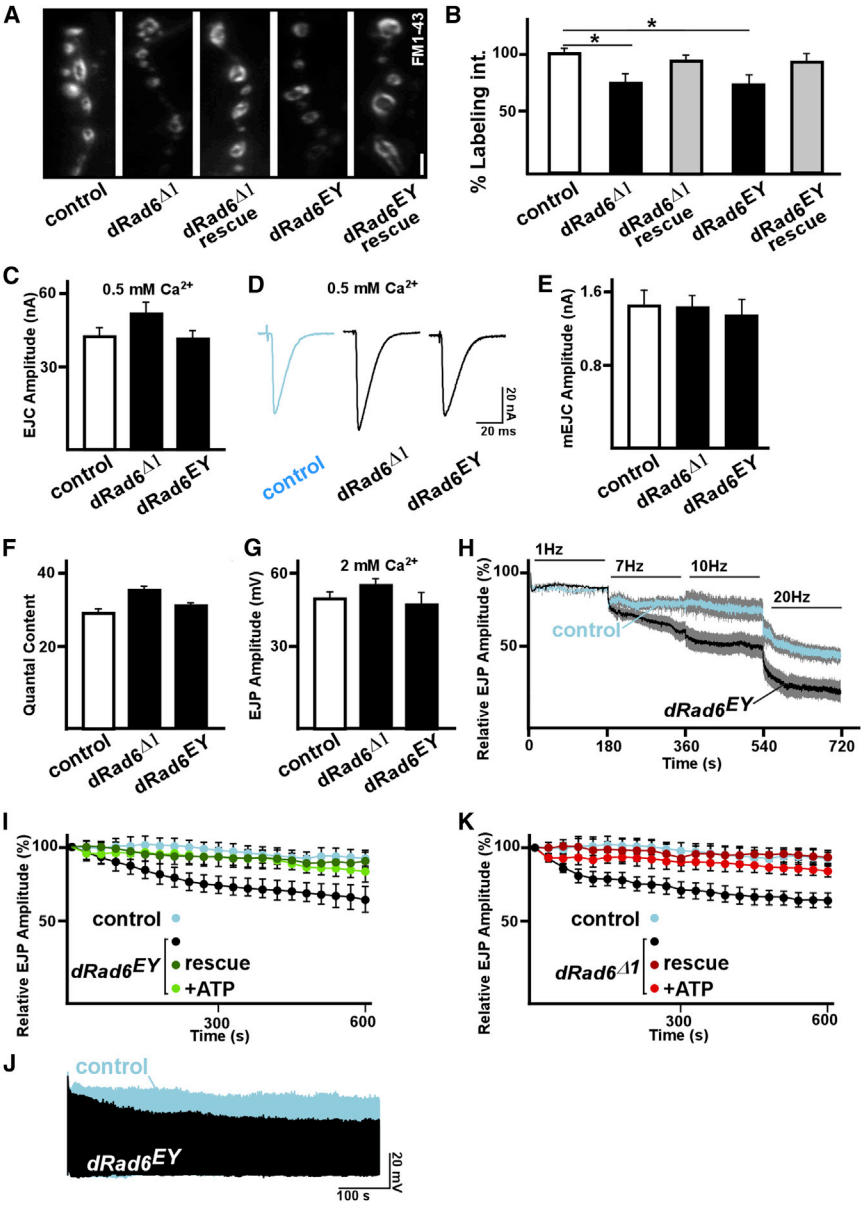

Figure 3. Synaptic Defects in *dRad6* Mutant Flies

(A and B) FM1-43 labeling at NMJ boutons of third instar larvae stimulated for 1 min using 90 mM KCl from controls, $dRad6^{\Delta 1}$ and $dRad6^{EY}$ mutants, and mutants that harbor a wild-type genomic dRAD6 construct (rescue) (scale bar = 4.5 μm) (A) and quantification normalized to control (B). Data are mean ± SEM, n = 6 animals; ANOVA post hoc Dunnett's test: *p < 0.05.

(C and D) Quantification of the average amplitude (C) of the EJC traces of recordings made at 1 Hz in 0.5 mM calcium (D) in control animals and in $dRad6^{\Delta 1}$ and $dRad6^{EY}$ mutant animals. Data are mean ± SEM; n = 8 animals; t test: ns, not significant.

(E and F) Quantification of the average mini EJC (mEJC) amplitude recorded in 0.5 mM calcium and TTX (E) and calculation of the quantal content (EJC/mEJC) (F). Data are mean ± SEM; n = 6 animals; t test: ns, not significant.

(G) Quantification of the average EJP amplitude of recordings made at 1 Hz (1 min) in 2 mM calcium in control animals and in $dRad6^{\Delta 1}$ and $dRad6^{EY}$ mutant animals. Data are mean ± SEM; n = 6 animals; t test: ns, not significant.

(H) Average EJP amplitude measured in HL-3 with 2 mM calcium when controls or $dRad6^{EY}$ mutants were sequentially stimulated at 1 Hz for 3 min, 7 Hz for 3 min, 10 Hz for 3 min, and 20 Hz for 3 min. n = 6 animals, and individual data points per animal were normalized to the first EJP amplitude measured at 1 Hz in that given animal and then averaged over the animals. Data are mean ± SEM.

(I) Average EJP amplitude upon stimulation at 10 Hz for 10 min in HL-3 with 2 mM calcium of control (blue), $dRad6^{EY}$ (black), $dRad6^{EY}$ mutants harboring a rescue construct (dark green), and $dRad6^{EY}$ mutants with motor neurons filled with ATP (light green). EJP amplitudes are binned per 30 s and normalized to the average of the first 15 s. Data are mean ± SEM; n = 6.

(J) Raw EJP traces of a 10 Hz 10 min recording in HL-3 with 2 mM calcium from control (light blue) and $dRad6^{EY}$ mutant (black).

(K) Average EJP amplitude upon stimulation at 10 Hz for 10 min in HL-3 with 2 mM calcium of control (blue), $dRad6^{\Delta 1}$ mutants (black), $dRad6^{\Delta 1}$ mutants harboring a rescue construct (dark red), and $dRad6^{\Delta 1}$ mutants with motor neurons filled with ATP (light red). EJP amplitudes are binned per 30 s and normalized to the average of the first 15 s. Data are mean ± SEM; n = 6.

mitochondrial protein ubiquitination (Lee et al., 2010), we tested the involvement of the RAD6A ubiquitin-conjugating enzyme in this process. We acutely induced mitophagy in control and *mRad6a* null MEFs using the mitochondrial uncoupler CCCP for 8 hr and determined protein ubiquitination in cytosolic and mitochondrial fractions using western blotting with anti-ubiquitin and with antibodies that recognize specific polyubiquitin chains linked at K48 and at K63 (Chan et al., 2011). The level of ubiquitination in the cytosolic fractions of CCCP-treated and dimethyl sulfoxide (DMSO)-treated samples does not differ between control and *mRad6a* null MEFs (Figures 4A and 4B). However, the level of total ubiquitin as well as K48-linked and K63-linked polyubiquitin in the mitochondrial fractions of CCCP-treated control MEFs is increased compared to control MEFs treated with DMSO (Figures 4A, asterisk, and 4B), in line with previous reports (Lee et al., 2010). In contrast, the level of total ubiquitination as well as K48-linked and K63-linked polyubiquitination in mitochondrial fractions of CCCP-treated *mRad6a* null MEFs does not significantly differ from the level of ubiquitination in DMSO-treated *mRad6a* null MEFs (Figures 4A and 4B). Thus, RAD6A is required for ubiquitination of mitochondrial proteins upon depolarization.

Ubiquitination marks mitochondria for degradation by several pathways, including autophagy (Chan et al., 2011). To test whether autophagy is altered in *mRad6a* null MEFs, we assessed the levels of p62/SQSTM1 (p62), an adaptor that recognizes

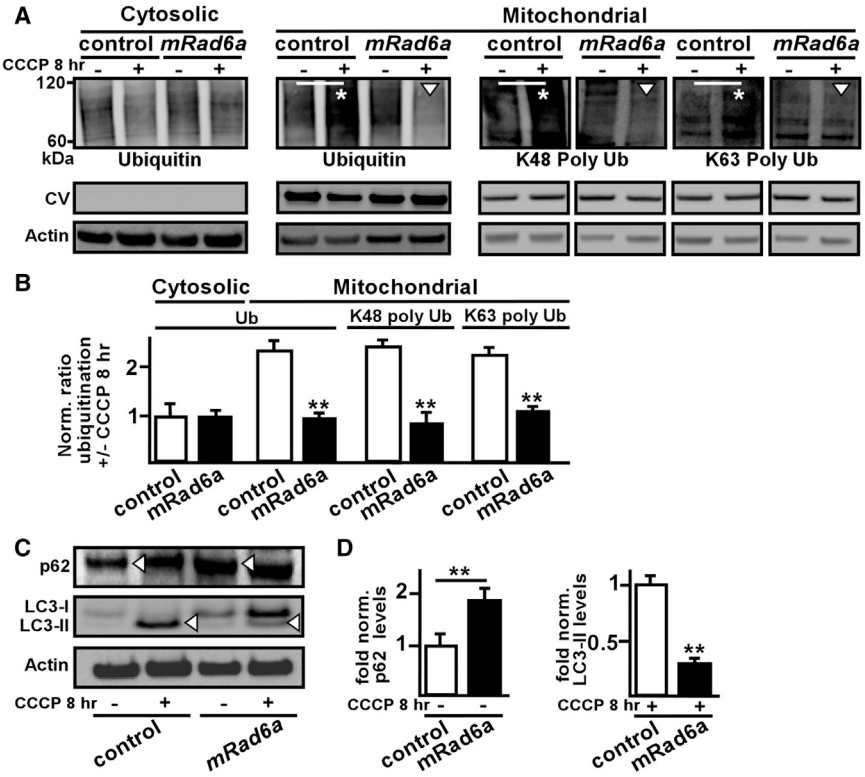

Figure 4. RAD6A Is Required for Ubiquitination of Mitochondrial Proteins and Autophagy

(A) Western blots of cytosolic and mitochondrial protein fractions from control and *mRad6a* null MEFs following CCCP or DMSO treatment probed with anti-ubiquitin, anti-K48-linkage- or anti-K63-linkage-specific polyubiquitin, anti-actin, or anti-CV (*, increased ubiquitination; arrowhead, ubiquitination levels are not affected in *mRad6a*$^{-/-}$ MEFs).

(B) Quantification of ubiquitination signal in CCCP- or DMSO-treated cells normalized to the ratio of CCCP or DMSO signal in control cytosol. Data are mean ± SEM for three experiments; t test: **$p < 0.01$.

(C and D) Western blots from control and *mRad6a* null MEFs treated with CCCP or DMSO for 8 hr and probed with anti-LC3 (LC3-II: compare arrowheads in +CCCP), anti-p62 (compare arrowheads in −CCCP), and anti-actin (C) and quantification of LC3-II and p62 levels (arrowheads) normalized to actin (D). Data are mean ± SEM for three experiments; t test: **$p < 0.01$.

ubiquitinated proteins and promotes the formation of autophagosomes that engulf damaged organelles, including mitochondria (McBride, 2008; Mizushima et al., 2011). A block in autophagy has been shown to correlate with an upregulation of p62 because cells treated with 3-MA, a compound that blocks the initiation of autophagy, as well as *ATG5*$^{-/-}$ and *ATG7*$^{-/-}$ knockout mouse cells that show reduced autophagy, both show increased levels of p62 (Klionsky et al., 2012; Komatsu et al., 2007; Tanabe et al., 2011). Similarly, we also found that p62 levels are significantly upregulated in *mRad6a* MEFs (Figures 4C, arrowhead, and 4D), consistent with a defect in autophagy.

Autophagosome formation requires the conversion of LC3-I to LC3-II and the binding of p62 to LC3 (Klionsky et al., 2012). Consistently, CCCP-induced mitochondrial depolarization promotes the conversion of LC3-I to LC3-II (Figures 4C and 4D) (Cai et al., 2012). Similarly, in CCCP-treated *mRad6a* knockout MEFs, the accumulation of LC3-II is much less pronounced than in CCCP-treated control cells (Figures 4C and 4D). These data are also in agreement with previous reports indicating that 3-MA trumps the accumulation of LC3-II (Tanabe et al., 2011), suggesting that, in *Rad6a* mutant cells, either the induction of autophagy is blocked or autophagic flux (LC3-II degradation) is facilitated.

RAD6A Facilitates CCCP-Induced Mitochondrial Clearance

If induction of autophagy is inhibited in *Rad6a* mutants, we expect mitochondria and mitochondrial proteins to accumulate upon CCCP treatment, whereas if clearance is facilitated, we expect organelles and proteins to be cleared faster. To assess mitophagic flux in *mRad6a* mutant cells, we first determined the abundance of different mitochondrial proteins using western blotting in cells treated for 8 hr with CCCP. While the levels of voltage-dependent anion channel 1 (VDAC1) and the beta subunit of complex V (CV), both mitochondrial proteins, are significantly reduced upon CCCP treatment of control MEFs compared to DMSO-treated MEFs (Figure 5A, arrowhead), we did not find a significant reduction in the levels of these proteins in *mRad6a* null MEFs (Figures 5A and 5B). These data argue against the idea that *Rad6a* mutant cells promote faster mitochondrial protein clearance upon CCCP treatment, suggesting rather that RAD6A is needed for the induction of autophagy (see below).

CCCP-uncoupled mitochondria also undergo morphological changes and are eventually cleared by mitophagy (Figure 5C, first column) (Geisler et al., 2010; Lee et al., 2010; Matsuda et al., 2010; Narendra et al., 2009; Rakovic et al., 2010; Vives-Bauza et al., 2010; Ziviani et al., 2010). Treatment of cells with 25 μM CCCP induces the formation of doughnut-like-shaped mitochondria (Liu and Hajnóczky, 2011). Next, mitochondrial proteins are ubiquitinated, leading to fragmentation, perinuclear clustering (before 8 hr of CCCP), and clearance (24 hr of CCCP) (Chan et al., 2011; Lee et al., 2010; Vives-Bauza et al., 2010). To determine if mRAD6A is required for mitochondrial clearance, we treated *mRad6a* null and control MEFs with 25 μM CCCP or DMSO and followed mitochondrial mass and morphology over a time period of 24 hr. While control MEFs treated with CCCP showed significant clearance of mitochondria after 24 hr (Figures 5C, second column, and 5D), most mitochondria in *mRad6a* null MEFs did not progress beyond the doughnut-like stage, nor were they cleared after 24 hr (Figures 5C, arrowhead and third column, and 5D). This defect is very similar to the block in

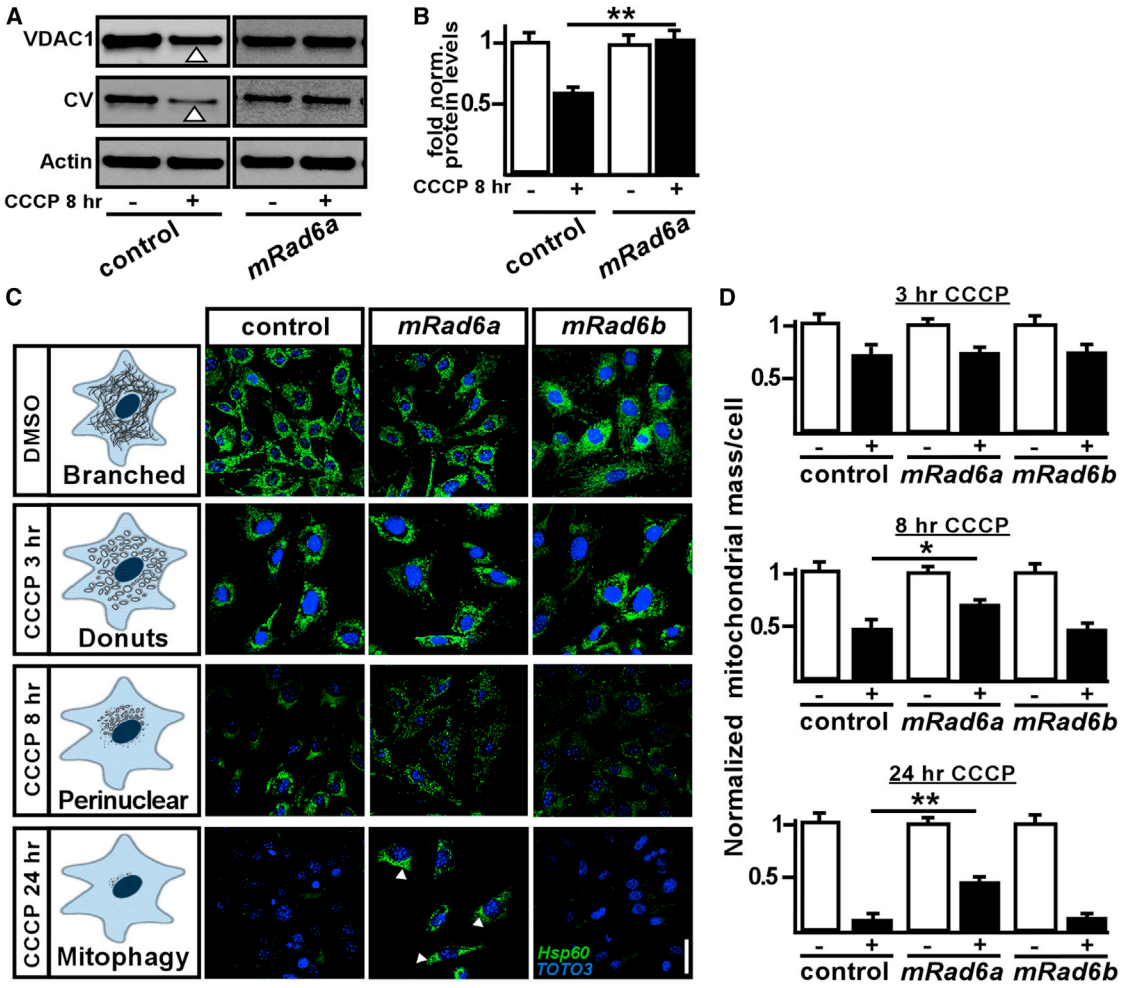

Figure 5. RAD6A Is Necessary for Efficient Mitochondrial Clearance

(A and B) Western blots from control and *mRad6a* null MEFs treated with CCCP or DMSO and probed with anti-VDAC1, anti-CV beta, and anti-actin (A) and quantification of protein levels normalized to actin (D). Data are mean ± SEM for three experiments; t test: **p < 0.01.

(C) Schematic of mitochondrial morphological changes and clearance upon CCCP treatment (first column) and images of the mitochondrial mass (labeled using anti-Hsp60) in control MEFs (second column), *mRad6a* null MEFs (third column), and *mRad6b* null MEFs (fourth column) subjected to DMSO treatment. TOTO-3 is a nuclear marker (scale bar = 40 μm). See also Figures S3A–S3F.

(D) Quantification of mitochondrial mass (Hsp60) normalized over cell area. Data are mean ± SEM; n = 30–50 cells from three experiments; ANOVA post hoc Dunnett's test: *p < 0.05, **p < 0.01.

mitochondrial clearance in CCCP-treated cells incubated with 3-MA (Figure S3A). The defect in mitochondrial clearance in *mRad6a* null MEFs is specific because mitochondria in CCCP-treated *mRad6b* null MEFs have a fate very similar to that of mitochondria of control MEFs, and most are cleared after 24 hr (Figures 5C, fourth column, and 5D). Furthermore, the defect in CCCP-induced mitochondrial clearance in *mRad6a* knockout MEFs is rescued when the cells are transfected either transiently with green fluorescent protein (GFP)-*hRad6a* (Figures 6A–6C) or stably with Myc-*mRad6a* (data not shown). Hence, *mRad6a* mutant cells display a defect to induce CCCP-dependent mitophagy.

Previous reports have shown that CCCP-induced mitophagy is mediated by the E3 ubiquitin ligase Parkin (Narendra et al., 2009); in a set of control experiments, we ascertained ourselves that the defect in mitochondrial clearance in *mRad6a* null MEFs is not the result of insufficient Parkin levels. First, while control MEFs in the presence of CCCP display obvious clearance of mitochondria in a 24 hr period, this process is largely inhibited in *Parkin* null MEFs (Figure S3B, fifth column). Second, we find *Parkin* gene expression in wild-type control MEFs and in *mRad6a* null MEFs by RT-PCR (Figure S3C). Third, mitophagy in *mRad6a* null cells that stably overexpress Parkin-GFP is still blocked (Figure S3D, bottom panels). In contrast, CCCP-depolarized mitochondria in wild-type MEFs that stably overexpress Parkin-GFP are efficiently cleared (Figure S3D, top panels). In addition, *mRad6a* null MEFs that stably express Parkin-GFP still display defects in autophagy (Figures S3E and S3F). Altogether, our data indicate an important role for RAD6A in clearing dysfunctional mitochondria.

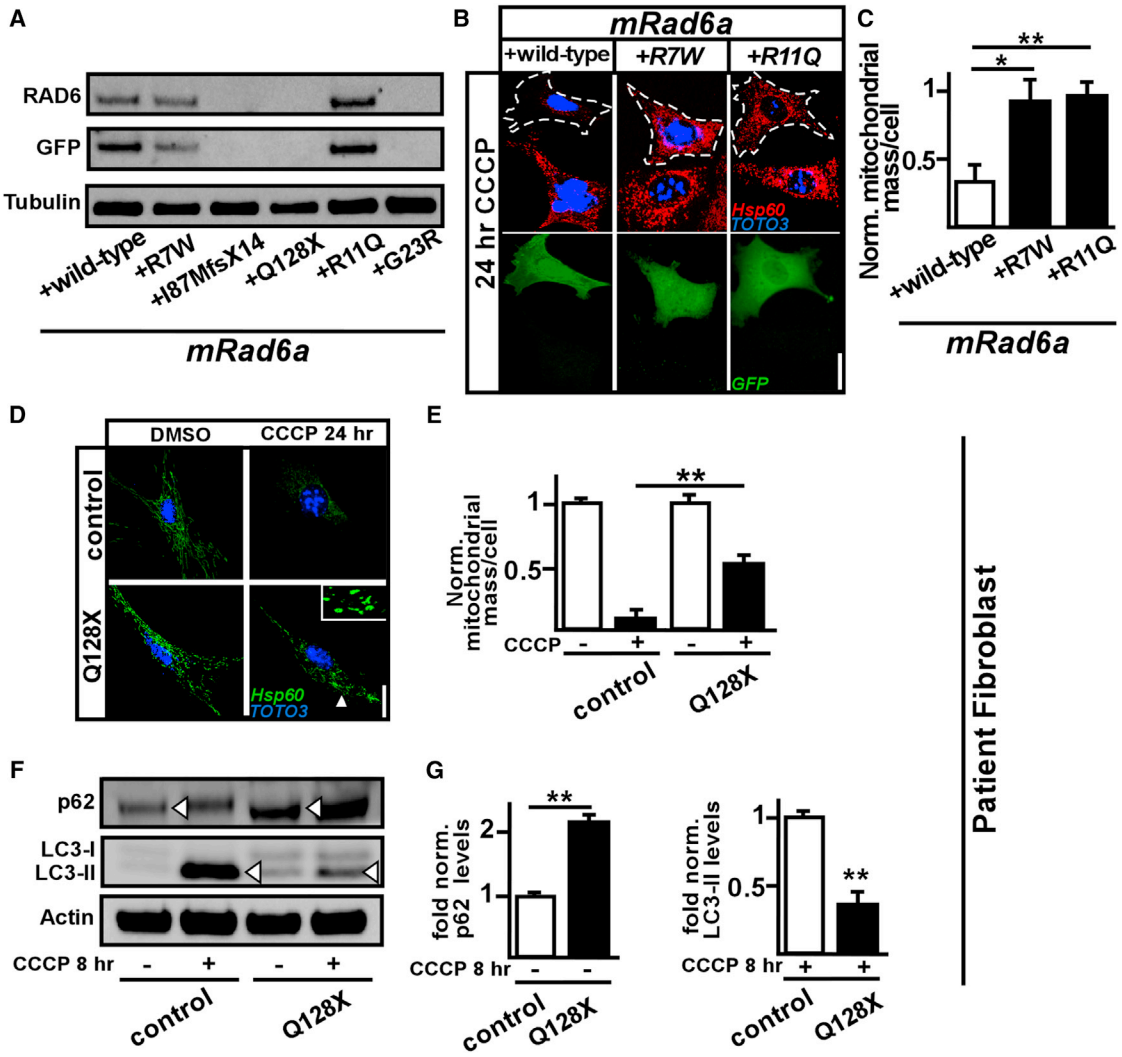

Figure 6. Clinical Mutations in *RAD6A* Do Not Support Mitophagy

(A) Western blots of *mRad6a* null MEFs transiently expressing wild-type hRAD6A and hRAD6A clinical mutants I87MfsX14, R7W, Q128X, R11Q, and G23R probed with anti-GFP, anti-RAD6A (N-terminal specific), and anti-Tubulin (three independent experiments).

(B) Images of mitochondrial mass (anti-Hsp60) in *mRad6a* null MEFs transiently expressing hRAD6A or clinical mutants (R7W or R11Q) following 24 hr of CCCP treatment. Transfected cells are labeled by anti-GFP, and nuclei are marked by TOTO-3 (scale bar = 8 μm).

(C) Quantification of mitochondrial mass. Data are mean ± SEM; n = at least 25 transfected cells from two experiments; t test: $^{**}p < 0.01$.

(D) Images of mitochondrial mass (anti-Hsp60) in control and patient-derived fibroblasts (Q128X) subjected to 24 hr DMSO or CCCP treatment. TOTO-3 is a nuclear marker. Scale bar = 8 μm.

(E) Quantification of mitochondrial mass. Data are mean ± SEM; n = 20 cells from two experiments; t test: $^{**}p < 0.01$.

(F) Western blots from control and patient-derived fibroblasts (Q128X) treated with CCCP or DMSO for 8 hr and probed with anti-LC3 (compare arrowheads in +CCCP), anti-p62 (compare arrowheads in −CCCP), and anti-actin.

(G) Quantification of LC3-II and p62 levels (arrowheads) normalized to actin. Data are mean ± SEM from three experiments; t test: $^{**}p < 0.01$. See also Figure S4.

Clinical *hRad6a* Mutants Do Not Support Mitophagy

To investigate the role of the ID-causing mutations in *hRad6a* at the level of mitophagy, we transiently expressed the clinical mutations we identified (I87MfsX14 and R7W) and the previously described mutations Q128X (Nascimento et al., 2006), R11Q, and G23R (Budny et al., 2010) tagged with GFP in *mRad6a* null MEFs. We first assessed expression of the mutant proteins and probed western blots of cellular extracts with anti-GFP and with N-terminal-specific RAD6A antibodies. In line with our inability to detect RAD6A in patient-derived cells, we were unable to detect hRAD6A in cells expressing I87MfsX14 (frameshift mutation leading to a deletion), Q128X (point mutation leading to a stop codon), and G23R (missense mutation leading to a predicted highly unstable protein; Budny et al., 2010) (Figure 6A). In contrast, we can detect wild-type hRAD6A as well as the R7W and R11Q mutants that harbor missense mutations affecting conserved amino acids at the N terminus (Figure 6A). Given that the hRAD6A R7W mutant protein is undetectable in

patient-derived cells (Figure 1), the data are consistent with the hRAD6A R7W protein being unstable and only detectable upon overexpression. It will be interesting to test if the R11Q mutation is detectable in patient-derived cells.

Next, to test if hRAD6A-R7W-GFP or hRAD6A-R11Q-GFP supports mitophagy, we incubated the *mRAD6A* null MEFs that express these mutants for 24 hr in CCCP. While *mRAD6A* null MEFs that express wild-type hRAD6A-GFP showed efficient clearance of mitochondria, *mRAD6A* null MEFs that express hRAD6A-R7W-GFP or hRAD6A-R11Q-GFP failed to efficiently degrade mitochondria (Figures 6B and 6C). Hence, while hRAD6A-R7W and hRAD6A-R11Q-GFP protein is detectable when overexpressed in *mRad6a* null cells, the mutant proteins are not able to promote CCCP-induced mitophagy.

Finally, we assessed if patient-derived fibroblasts carrying the Q128X mutation display mitochondrial clearance when incubated in CCCP. As shown in Figures 6D (arrowhead) and 6E, mitophagy is much reduced in the patient-derived cells compared to control cells. In line with defects in autophagy, the patient-derived fibroblasts also display reduced LC3-II levels upon CCCP treatment and show a concomitant accumulation of p62 levels (Figures 6F and 6G). Hence, cells with hRAD6A clinical mutants show a defect to promote CCCP-induced mitochondrial clearance.

RAD6A Is a Parkin E2 Ubiquitin-Conjugating Enzyme

Several E3 ubiquitin ligases have been described as acting with RAD6A in the nucleus, including Rad18, Ubr1, and Bre1 (Game and Chernikova, 2009). To test if these E3 ubiquitin ligases are involved in the control of mitochondrial function, we knocked down Ubr1 and Bre1 (fruit flies do not harbor a Rad18 homolog) using RNAi in fruit flies (Figure S4A). As a control, we also knocked down Parkin. Knockdown of Bre1 in fruit flies results in embryonic lethality, precluding us from analyzing JC-1 labeling in larval motor neurons. While knockdown of Parkin results in reduced red JC-1 labeling, indicating a less-negative $\Delta\psi m$, knockdown of Ubr1 has no effect (Figures S4B and S4C). Similarly, we used GFP-labeled small hairpin RNA (shRNA) to knock down Ubr1, Rad18, or Bre1 in mammalian cells (Figures S4D and S4E) and tested if knockdown of these E3 ligases affected mitochondrial clearance upon CCCP treatment of the cells. In contrast to Parkin mutant MEFs (Figure S3B), MEFs with reduced levels of Rad18, Ubr1, or Bre1 efficiently cleared their mitochondria following CCCP treatment, very similar to untransfected control cells in CCCP (Figures S4F and S4G). Hence, three of the E3 ubiquitin ligases that are known to operate with RAD6A in the nucleus do not affect mitochondrial function.

As previously shown, Parkin is an E3 ubiquitin ligase involved in the ubiquitination of mitochondrial proteins and mitophagy (Lee et al., 2010) (Figure S3). In cells, loss of Parkin blocks CCCP-induced mitophagy (Figure S3B). In flies, *parkin* mutant motor neurons harbor mitochondria with a less-negative $\Delta\psi m$ (Figures S4B and S4C) and *parkin* mutant muscles harbor enlarged and doughnut-shaped morphologically abnormal mitochondria (Figure S4H). These phenotypes, including the mitochondrial morphological defects in muscles, are all very reminiscent of those seen in Rad6a mutant cells and flies (Figures 2, 5, 6, and S4H). We therefore tested the hypothesis that RAD6A serves as an E2 ubiquitin-conjugating enzyme that can act with Parkin. First, we performed an in vitro ubiquitination assay (Hristova et al., 2009) using 90 nM purified recombinant E1, 2.5 μM hRAD6A, 3 μM Parkin, and 0.2 mM ubiquitin (Figures 7A and S5A). Probing reactions that include the E1, hRAD6A, Parkin, and ubiquitin with anti-ubiquitin reveal ubiquitination that is not obvious when either protein is omitted (Figure 7A). Furthermore, we also performed a more sensitive ELISA-based in vitro ubiquitination assay (Marblestone et al., 2010) and incubated different concentrations of hRAD6A with 60 nM Parkin, 5 nM E1 activating enzyme, and 9 mM ubiquitin. We then quantitatively assessed newly synthesized ubiquitin chain formation by measuring luminescence. While hRAD6A alone is not able to form a significant amount of ubiquitin chains (Figure 7B), hRAD6A and Parkin together are very effective in forming ubiquitin chains in a hRAD6A dose-dependent manner. The in vitro ubiquitination assay reveals significant enzymatic activity of hRAD6A toward Parkin, since adding a known Parkin E2 ubiquitin-conjugating enzyme (UBCH7) (Tanaka et al., 2001) is less effective at forming ubiquitin chains than hRAD6A in a similar concentration range (Figure 7C). We fitted the data using a Michaelis-Menten kinetics model and calculated the apparent K_M (nM) values for the Parkin-dependent ubiquitination reaction mediated by hRAD6A (Figure 7D). These data indicate that Parkin and hRAD6A can form a functional ubiquitination partnership in vitro and suggest that RAD6A can be a cognate E2 ubiquitin-conjugating enzyme for the E3 ubiquitin ligase Parkin.

Next, we tested if RAD6A and Parkin interact in a cell-based assay. Parkin is implicated in mediating mitophagy upon translocation to depolarized mitochondria that are destined for degradation (Narendra et al., 2009). We therefore assessed if an interaction between the two proteins would be affected by mitochondrial depolarization. For this, we immunoprecipitated Parkin from MEFs stably expressing Parkin-GFP (Figures S5B and S5C) following a 6 hr treatment with CCCP. Western blots probed with anti-RAD6A antibody revealed that Parkin coimmunoprecipitates with RAD6A and that RAD6A and Parkin binding is increased upon mitochondrial uncoupling (Figure 7E, lower panel), indicating that the two proteins interact upon mitochondrial depolarization.

Assessing the functionality of the RAD6A-Parkin interaction, we tested if autoubiquitination of Parkin requires RAD6A. Parkin-GFP autoubiquitination is dramatically induced upon mitochondrial depolarization (Matsuda et al., 2010; Tanaka et al., 2010). We therefore immunoprecipitated Parkin from control and *mRad6a* null MEFs treated for 6 hr with DMSO or CCCP and probed the same western blots for Parkin (Figures 7E and S5D) and ubiquitin (Figure 7F). While we observed an obvious Parkin laddering pattern (Figures 7E and S5D) that is also ubiquitin positive in CCCP-treated control cells (Figure 7F), this pattern is not as prevalent in *mRad6a* null MEFs (Figures 7E and 7F). Indicating specificity, immunoprecipitations (IPs) using nonspecific immunoglobulin G (IgG) antibodies did not reveal Parkin or ubiquitin-positive signals. Thus, RAD6A facilitates Parkin autoubiquitination upon mitochondrial depolarization.

Finally, to test if Parkin relocalization to depolarized mitochondria is RAD6A dependent, we treated Parkin-GFP expressing

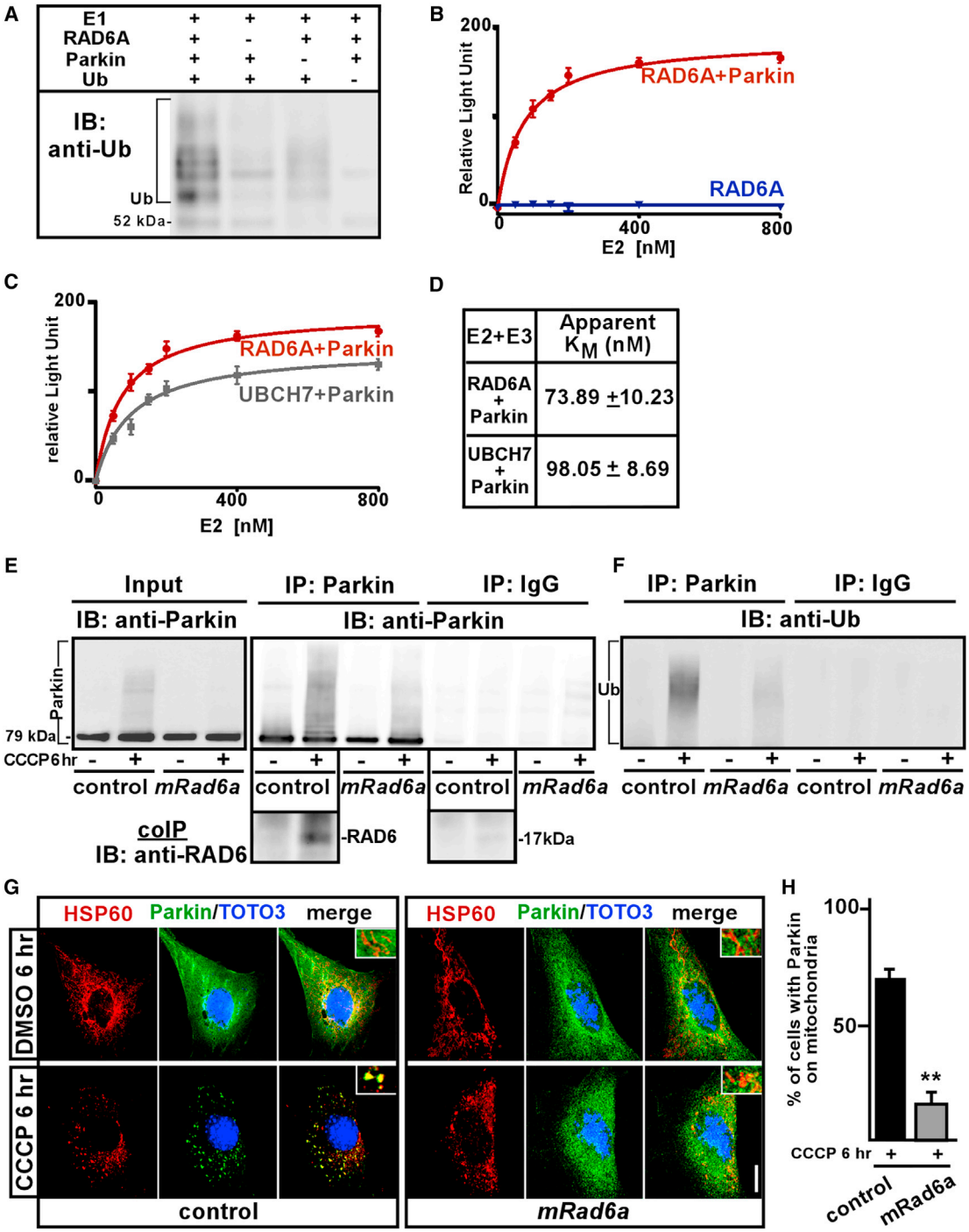

Figure 7. RAD6A Is an E2 Ubiquitin-Conjugating Enzyme for Parkin

(A) Western blot of in vitro ubiquitination assay using the proteins indicated and probed with anti-ubiquitin antibody (two experiments). See also Figure S4.

(B and C) ELISA-based in vitro ubiquitination assay using RAD6A, Parkin, and E1 (B) and UBCH7, Parkin, and E1 (C) (related to Figure S5A).

(D) Calculation of apparent K_M (nM) using a Michaelis-Menten kinetics model. Data are mean ± SEM for three experiments.

(E and F) Western blots of IPs of Parkin-GFP using anti-GFP antibody or IgG control from DMSO (–)- or CCCP (+)-treated control or *mRad6a* knockout MEFs expressing Parkin-GFP and probed with anti-Parkin (upper panel), anti-RAD6 (lower panel) (E) or anti-ubiquitin (F). See also Figures S5B–S5D.

(G) Labeling of DMSO- or CCCP-treated control or *mRad6a* knockout MEFs expressing Parkin-GFP, using anti-Hsp60 (a mitochondrial marker) and anti-GFP (to label Parkin) (scale bar = 8 μm); insets show enlarged view of mitochondria.

(H) Quantification of the number of cells in which Parkin is relocalized to mitochondria. See also Figure S5E. Data are mean ± SEM; n = 30 cells for three experiments; t test: $^{**}p < 0.01$.

control and *mRad6a* null MEFs with CCCP or DMSO for 6 hr and determined the subcellular localization of Parkin (Figures 7G, 7H, and S5E). While Parkin translocates from its diffuse cytosolic localization to mitochondria in control MEFs upon CCCP treatment, it fails to do so appreciably in *mRad6*a null MEFs (Figures 7G, 7H, and S5D), suggesting that Parkin translocation to depolarized mitochondria is critically dependent on RAD6A. Taken together, our data indicate that RAD6A and Parkin form a functional E2/E3 ubiquitination pair that mediates mitophagy.

DISCUSSION

In this study, we identified two families with mutations in the XLID-associated protein RAD6A. Further investigation of the functional implications of those mutations led to the unexpected finding that RAD6A has a central role in triggering mitophagy upon mitochondrial depolarization in cells and is required to maintain mitochondrial integrity in vivo. Although a direct involvement of mitophagy in mitochondrial quality control in vivo is debated, disruption of the process is thought to result in the gradual age-dependent accumulation of dysfunctional mitochondria (Mizushima and Komatsu, 2011). Given that a healthy mitochondrial pool is critical not only for neuronal communication (Kang et al., 2008; Morais et al., 2009; Sheng and Cai, 2012; Verstreken et al., 2005), but also for normal spine morphogenesis in the postsynaptic compartment (Li et al., 2004), our findings link a cytoplasmic role of RAD6A at the level of mitochondria to synaptic function. This conclusion is supported by electrophysiological analyses in *dRad6* loss-of-function fly mutants that display reduced synaptic transmission during intense stimulation and are largely rescued by supplying extra ATP. Further studies are now required to assess which neurons are most affected in the human brain. Interestingly, loss of RAD6B, a closely related isoform, does not affect mitochondrial integrity, and mutations in RAD6B have never been found in intellectually disabled patients. Without excluding additional roles for RAD6A, our work is consistent with a model in which the cellular and neuronal dysfunction upon loss of RAD6A function is at least in part caused by dysfunctional mitochondria.

Disturbed mitophagy has been linked to Parkin, an E3 ubiquitin ligase, and mutations in *parkin* cause juvenile Parkinsonism. Parkin is thought to ubiquitinate mitochondrial proteins (Chan et al., 2011; Lee et al., 2010); however, E2 ubiquitin-conjugating enzymes that mediate Parkin translocation to mitochondria in response to their depolarization have not yet been identified. Our data suggest that RAD6A is an E2 enzyme that can operate with the E3 ligase Parkin upon mitochondrial depolarization to induce mitochondrial ubiquitination. As ID patients do not display overt Parkinsonism, we speculate that other E2 conjugating enzymes may be involved in Parkin-dependent ubiquitination in the neurons of the *substantia nigra*, providing compensation in the brain regions responsible for Parkinson's disease (PD)-related symptoms. Conversely, RAD6A can transfer ubiquitin to different E3s besides Parkin (Game and Chernikova, 2009); therefore, the situation in different brain regions is more complex and will need careful scrutiny. We anticipate that in brain regions where RAD6A is highly expressed together with Parkin, for instance in the dorsolateral prefrontal cortex (Kupershmidt et al., 2010), both proteins might interact. In other brain regions, this is likely different; for instance, RAD6A is only weakly present in the *substantia nigra*, a location where Parkin is strongly expressed (Kupershmidt et al., 2010). Thus, different neurons in the brain may be differentially dependent on RAD6A function.

Defects in autophagy and in mitochondrial function are implicated in diverse processes, such as brain development, synaptic function, neuronal differentiation, and aging (Ishihara et al., 2009; Kageyama et al., 2012; Le Bot, 2007; Wirawan et al., 2012), where alterations in reactive oxygen species (ROS) homeostasis and redox regulation, in part induced by an accumulation of dysfunctional mitochondria, may be the culprit in a wide spectrum of neuronal diseases (Kirkinezos and Moraes, 2001; Oikawa et al., 2012; Ray et al., 2012; Sabens Liedhegner et al., 2012). Interestingly, in cortical neuron cultures, *Rad6a* levels are upregulated in response to oxidative stress (Shalamanova et al., 2007), particularly to hypochlorous acid (HOCl), one of the major oxidants (Higgins et al., 2010). These findings are consistent with a model in which RAD6A plays an important role in mitigating oxidative stress response to maintain a healthy population of mitochondria. In conclusion, our work links XLID-associated defects caused by RAD6A mutations to mitochondrial deficits and neuronal dysfunction.

EXPERIMENTAL PROCEDURES

Genetics

Identification of the *Ube2a* mutations identified in this study and patient features are in the Supplemental Experimental Procedures and Table S1. The work in this paper was approved by the ethical review board of KU Leuven, and patient material was obtained with the consent of the patients or their legal guardians. UAS-RNAi lines (Dietzl et al., 2007) (Table S2) and y^1 w^{67c23}; *P{EPgy2}UbcD6*^{EY04634} (Bellen et al., 2011) were from the Vienna *Drosophila* RNAi Center (VDRC) and the Bloomington stock center. *dRad6*$^{\Delta 1}$ was generated by P element excision (Supplemental Experimental Procedures), and both alleles were backcrossed several times to y^1 w^{67c23}. Germline transformation of genomic *dRad6* (BAC CH322-46G02) (*dRad6*$^+$) in the VK37 docking site was obtained using PhiC31-mediated integration (GenetiVision).

Cell Lines and Plasmids

Immortalized control (*mRad6a/b*$^{+/+}$) and *mRad6a* null (*mRad6a*$^{-/-}$) MEFs were obtained from W. Baarends (EMC) (Roest et al., 2004), and human fibroblasts harboring a *hRad6a* Q128X mutation were described (Nascimento et al., 2006). Immortalized control (*mParkin*$^{+/+}$) and *mParkin* null (*mParkin*$^{-/-}$) MEFs were obtained from K. Winklhofer (Ludwig Maximilian University of Munich). Generation of stable and transient transfected cell lines is described in the Supplemental Experimental Procedures.

Fluorescence Imaging

Ψm in *Drosophila* NMJ mitochondria was assessed using JC-1 (Molecular Probes) (Morais et al., 2009). TMRE (Molecular Probes) labeling was adapted from Narendra et al. (2009). FM1-43 labeling at third instar NMJs was performed as described (Verstreken et al., 2008). Antibodies for immunohistochemistry and imaging conditions are listed in the Supplemental Experimental Procedures.

Electrophysiology

EJCs or EJPs in HL-3 with $CaCl_2$ from muscle 6 in segment A2 or A3 were performed as described (Uytterhoeven et al., 2011). Motor nerves were

stimulated at 2× threshold, and intracellular electrodes had resistances <10 MΩ. For TEVC, the holding potential was −70 mV and input resistances were >5 MΩ. Data were acquired and digitized using an Axoclamp 900A Amplifier, a Digidata 1440A, and pCLAMP 10 (Molecular devices). Motor neurons were forward filled with 1 mM ATP as described (Verstreken et al., 2005).

Biochemistry

Protein extracts were processed for IEF/SDS-PAGE according to the ZOOM IPGRunner system protocol (Invitrogen). Protein extracts (25–75 μg) resuspended in 8 M urea, 2 M thiourea, 2% CHAPS, 20 mM dithiothreitol (DTT), 0.5% (v/v) ZOOM Carrier Ampholytes were loaded on a pH 4–7 ZOOM Strip. Immobilized pH gradient (IPG) strips were rehydratated for 16 hr at 20°C. The first dimension that consisted of isoelectrical focusing (IEF) was performed at 1 mA/strip. Each strip was equilibrated with NuPAGE LDS Sample Buffer containing 10 mg/ml DTT for 15 min followed by buffer containing 25 mg/ml iodoacetamide for 15 min. Strips were then loaded and analyzed on a 4%–12% Bis-Tris ZOOM Gel at 170 V for 35 min. For subcellular fractionations, cells were collected in 0.2 M sucrose, 10 mM Tris-MOPS (pH 7.4), 0.1 mM EGTA-Tris (pH 7.4) and then disrupted using a Teflon homogenizer at 1,000 rpm for 30 strokes. Homogenates were centrifuged at 800 × *g* for 10 min, and supernatants were centrifuged again at 7,000 × *g* for 10 min. Pellets were resuspended and proteins detected by western blot. For autoubiquitination, the assay based on western blotting was adapted from Hristova et al. (2009). In vitro ubiquitination based on ELISA was performed using the E2 Profiling Kit (LifeSensors). IPs, including the protein extraction and detection, were performed by standard protocols (Van Humbeeck et al., 2011). Cells were lysed in 50 mM Tris-HCl (pH 7.4), 150 mM NaCl, 1% Triton X-100, and Complete protease inhibitor (Roche Applied Science) and incubated with anti-GFP antibody for 2 hr, then coupled to protein G beads for 1 hr. IPs were washed with lysis buffer, eluted directly into SDS-PAGE sample buffer, and detected by western blot. Antibodies and primers used for RT-PCR are listed in the Supplemental Experimental Procedures.

Statistics

The statistical significance of differences between a set of two groups was evaluated using unpaired t tests (*$p < 0.05$; **$p < 0.01$) and between more than two groups using one-way ANOVA ($p < 0.01$) and Dunnett's test (*$p < 0.05$; **$p < 0.01$) in GraphPad Prism 5.

SUPPLEMENTAL INFORMATION

Supplemental Information includes five figures, two tables, and Supplemental Experimental Procedures and can be found with this article online at http://dx.doi.org/10.1016/j.molcel.2013.04.012.

ACKNOWLEDGMENTS

We thank the Bloomington and VDRC stock centers; Kyoung Sang Cho, Willy Baarends, and Konstanze Winklhofer for reagents; and Bassem Hassan, Wim Vandenberghe, and members of the Verstreken and De Strooper labs for comments. V.M.K. is financed by a grant of the German Ministry of Education and Research through the MRNET and by the Project GENCODYS (241995), which is funded by the European Union Framework Program 7 (FP7); S.V. and M.L. are supported by an FWO postdoctoral fellowship; and M.V. is supported by an IWT predoctoral fellowship and a PDM postdoctoral fellowship by the research fund KU Leuven. Support to P.V. was provided by a Marie Curie Excellence Grant (MEXT-CT-2006-042267), an ERC Starting Grant (260678), the Research Foundation Flanders (FWO grants G053913, G079013, G095511, and G074709), a Methusalem grant of the Flemish Government, the Francqui Foundation, the Hercules Foundation (AKUL/09/037), the Instutuut voor Wetenschap en Technologie (IWT), the Interuniversity Attraction Pole program by BELSPO (IAP P7/16 NEUROBRAINNET), the research fund KU Leuven (OT Start, GOA/13/017), and VIB.

Received: September 4, 2012
Revised: February 19, 2013
Accepted: April 10, 2013
Published: May 16, 2013

REFERENCES

Backx, L., Vermeesch, J., Pijkels, E., de Ravel, T., Seuntjens, E., and Van Esch, H. (2010). PPP2R2C, a gene disrupted in autosomal dominant intellectual disability. Eur. J. Med. Genet. *53*, 239–243.

Baker, K., Raymond, F.L., and Bass, N. (2012). Genetic investigation for adults with intellectual disability: opportunities and challenges. Curr. Opin. Neurol. *25*, 150–158.

Bellen, H.J., Levis, R.W., He, Y., Carlson, J.W., Evans-Holm, M., Bae, E., Kim, J., Metaxakis, A., Savakis, C., Schulze, K.L., et al. (2011). The Drosophila gene disruption project: progress using transposons with distinctive site specificities. Genetics *188*, 731–743.

Budny, B., Badura-Stronka, M., Materna-Kiryluk, A., Tzschach, A., Raynaud, M., Latos-Bielenska, A., and Ropers, H.H. (2010). Novel missense mutations in the ubiquitination-related gene UBE2A cause a recognizable X-linked mental retardation syndrome. Clin. Genet. *77*, 541–551.

Cai, Q., Zakaria, H.M., Simone, A., and Sheng, Z.H. (2012). Spatial parkin translocation and degradation of damaged mitochondria via mitophagy in live cortical neurons. Curr. Biol. *22*, 545–552.

Chan, D.C. (2006). Mitochondria: dynamic organelles in disease, aging, and development. Cell *125*, 1241–1252.

Chan, N.C., Salazar, A.M., Pham, A.H., Sweredoski, M.J., Kolawa, N.J., Graham, R.L., Hess, S., and Chan, D.C. (2011). Broad activation of the ubiquitin-proteasome system by Parkin is critical for mitophagy. Hum. Mol. Genet. *20*, 1726–1737.

de Leeuw, N., Bulk, S., Green, A., Jaeckle-Santos, L., Baker, L.A., Zinn, A.R., Kleefstra, T., van der Smagt, J.J., Vianne Morgante, A.M., de Vries, B.B., et al. (2010). UBE2A deficiency syndrome: Mild to severe intellectual disability accompanied by seizures, absent speech, urogenital, and skin anomalies in male patients. Am. J. Med. Genet. A. *152A*, 3084–3090.

Dickman, D.K., Horne, J.A., Meinertzhagen, I.A., and Schwarz, T.L. (2005). A slowed classical pathway rather than kiss-and-run mediates endocytosis at synapses lacking synaptojanin and endophilin. Cell *123*, 521–533.

Dietzl, G., Chen, D., Schnorrer, F., Su, K.C., Barinova, Y., Fellner, M., Gasser, B., Kinsey, K., Oppel, S., Scheiblauer, S., et al. (2007). A genome-wide transgenic RNAi library for conditional gene inactivation in Drosophila. Nature *448*, 151–156.

Game, J.C., and Chernikova, S.B. (2009). The role of RAD6 in recombinational repair, checkpoints and meiosis via histone modification. DNA Repair (Amst.) *8*, 470–482.

Geisler, S., Holmström, K.M., Skujat, D., Fiesel, F.C., Rothfuss, O.C., Kahle, P.J., and Springer, W. (2010). PINK1/Parkin-mediated mitophagy is dependent on VDAC1 and p62/SQSTM1. Nat. Cell Biol. *12*, 119–131.

Higgins, G.C., Beart, P.M., Shin, Y.S., Chen, M.J., Cheung, N.S., and Nagley, P. (2010). Oxidative stress: emerging mitochondrial and cellular themes and variations in neuronal injury. J. Alzheimers Dis. *20*(*Suppl 2*), S453–S473.

Honda, S., Orii, K.O., Kobayashi, J., Hayashi, S., Imamura, A., Imoto, I., Nakagawa, E., Goto, Y., and Inazawa, J. (2010). Novel deletion at Xq24 including the UBE2A gene in a patient with X-linked mental retardation. J. Hum. Genet. *55*, 244–247.

Hristova, V.A., Beasley, S.A., Rylett, R.J., and Shaw, G.S. (2009). Identification of a novel Zn2+-binding domain in the autosomal recessive juvenile Parkinson-related E3 ligase parkin. J. Biol. Chem. *284*, 14978–14986.

Ishihara, N., Nomura, M., Jofuku, A., Kato, H., Suzuki, S.O., Masuda, K., Otera, H., Nakanishi, Y., Nonaka, I., Goto, Y., et al. (2009). Mitochondrial fission factor Drp1 is essential for embryonic development and synapse formation in mice. Nat. Cell Biol. *11*, 958–966.

Jentsch, S., McGrath, J.P., and Varshavsky, A. (1987). The yeast DNA repair gene RAD6 encodes a ubiquitin-conjugating enzyme. Nature *329*, 131–134.

Kageyama, Y., Zhang, Z., Roda, R., Fukaya, M., Wakabayashi, J., Wakabayashi, N., Kensler, T.W., Reddy, P.H., Iijima, M., and Sesaki, H. (2012). Mitochondrial division ensures the survival of postmitotic neurons by suppressing oxidative damage. J. Cell Biol. *197*, 535–551.

Kang, J.S., Tian, J.H., Pan, P.Y., Zald, P., Li, C., Deng, C., and Sheng, Z.H. (2008). Docking of axonal mitochondria by syntaphilin controls their mobility and affects short-term facilitation. Cell *132*, 137–148.

Karras, G.I., and Jentsch, S. (2010). The RAD6 DNA damage tolerance pathway operates uncoupled from the replication fork and is functional beyond S phase. Cell *141*, 255–267.

Kirkinezos, I.G., and Moraes, C.T. (2001). Reactive oxygen species and mitochondrial diseases. Semin. Cell Dev. Biol. *12*, 449–457.

Klionsky, D.J., Abdalla, F.C., Abeliovich, H., Abraham, R.T., Acevedo-Arozena, A., Adeli, K., Agholme, L., Agnello, M., Agostinis, P., Aguirre-Ghiso, J.A., et al. (2012). Guidelines for the use and interpretation of assays for monitoring autophagy. Autophagy *8*, 445–544.

Koken, M.H., Reynolds, P., Jaspers-Dekker, I., Prakash, L., Prakash, S., Bootsma, D., and Hoeijmakers, J.H. (1991). Structural and functional conservation of two human homologs of the yeast DNA repair gene RAD6. Proc. Natl. Acad. Sci. USA *88*, 8865–8869.

Koken, M.H., Hoogerbrugge, J.W., Jasper-Dekker, I., de Wit, J., Willemsen, R., Roest, H.P., Grootegoed, J.A., and Hoeijmakers, J.H. (1996). Expression of the ubiquitin-conjugating DNA repair enzymes HHR6A and B suggests a role in spermatogenesis and chromatin modification. Dev. Biol. *173*, 119–132.

Komatsu, M., Waguri, S., Koike, M., Sou, Y.S., Ueno, T., Hara, T., Mizushima, N., Iwata, J., Ezaki, J., Murata, S., et al. (2007). Homeostatic levels of p62 control cytoplasmic inclusion body formation in autophagy-deficient mice. Cell *131*, 1149–1163.

Kupershmidt, I., Su, Q.J., Grewal, A., Sundaresh, S., Halperin, I., Flynn, J., Shekar, M., Wang, H., Park, J., Cui, W., et al. (2010). Ontology-based meta-analysis of global collections of high-throughput public data. PLoS ONE *5*, 5.

Le Bot, N. (2007). Autophagy: a new regulator of development. Nat. Cell Biol. *9*, 741.

Lee, K.Y., and Myung, K. (2008). PCNA modifications for regulation of post-replication repair pathways. Mol. Cells *26*, 5–11.

Lee, J.Y., Nagano, Y., Taylor, J.P., Lim, K.L., and Yao, T.P. (2010). Disease-causing mutations in parkin impair mitochondrial ubiquitination, aggregation, and HDAC6-dependent mitophagy. J. Cell Biol. *189*, 671–679.

Li, Z., Okamoto, K., Hayashi, Y., and Sheng, M. (2004). The importance of dendritic mitochondria in the morphogenesis and plasticity of spines and synapses. Cell *119*, 873–887.

Liu, X., and Hajnóczky, G. (2011). Altered fusion dynamics underlie unique morphological changes in mitochondria during hypoxia-reoxygenation stress. Cell Death Differ. *18*, 1561–1572.

Marblestone, J.G., Suresh Kumar, K.G., Eddins, M.J., Leach, C.A., Sterner, D.E., Mattern, M.R., and Nicholson, B. (2010). Novel approach for characterizing ubiquitin E3 ligase function. J. Biomol. Screen. *15*, 1220–1228.

Martin, I., Dawson, V.L., and Dawson, T.M. (2011). Recent advances in the genetics of Parkinson's disease. Annu. Rev. Genomics Hum. Genet. *12*, 301–325.

Matsuda, N., Sato, S., Shiba, K., Okatsu, K., Saisho, K., Gautier, C.A., Sou, Y.S., Saiki, S., Kawajiri, S., Sato, F., et al. (2010). PINK1 stabilized by mitochondrial depolarization recruits Parkin to damaged mitochondria and activates latent Parkin for mitophagy. J. Cell Biol. *189*, 211–221.

McBride, H.M. (2008). Parkin mitochondria in the autophagosome. J. Cell Biol. *183*, 757–759.

Mizushima, N., and Komatsu, M. (2011). Autophagy: renovation of cells and tissues. Cell *147*, 728–741.

Mizushima, N., Yoshimori, T., and Ohsumi, Y. (2011). The role of Atg proteins in autophagosome formation. Annu. Rev. Cell Dev. Biol. *27*, 107–132.

Morais, V.A., Verstreken, P., Roethig, A., Smet, J., Snellinx, A., Vanbrabant, M., Haddad, D., Frezza, C., Mandemakers, W., Vogt-Weisenhorn, D., et al. (2009). Parkinson's disease mutations in PINK1 result in decreased Complex I activity and deficient synaptic function. EMBO Mol Med *1*, 99–111.

Narendra, D., Tanaka, A., Suen, D.F., and Youle, R.J. (2009). Parkin-induced mitophagy in the pathogenesis of Parkinson disease. Autophagy *5*, 706–708.

Nascimento, R.M., Otto, P.A., de Brouwer, A.P., and Vianna-Morgante, A.M. (2006). UBE2A, which encodes a ubiquitin-conjugating enzyme, is mutated in a novel X-linked mental retardation syndrome. Am. J. Hum. Genet. *79*, 549–555.

Oikawa, D., Akai, R., Tokuda, M., and Iwawaki, T. (2012). A transgenic mouse model for monitoring oxidative stress. Sci Rep *2*, 229.

Prakash, L. (1994). The RAD6 gene and protein of Saccharomyces cerevisiae. Ann. N Y Acad. Sci. *726*, 267–273.

Rakovic, A., Grünewald, A., Seibler, P., Ramirez, A., Kock, N., Orolicki, S., Lohmann, K., and Klein, C. (2010). Effect of endogenous mutant and wild-type PINK1 on Parkin in fibroblasts from Parkinson disease patients. Hum. Mol. Genet. *19*, 3124–3137.

Ray, P.D., Huang, B.W., and Tsuji, Y. (2012). Reactive oxygen species (ROS) homeostasis and redox regulation in cellular signaling. Cell. Signal. *24*, 981–990.

Roest, H.P., Baarends, W.M., de Wit, J., van Klaveren, J.W., Wassenaar, E., Hoogerbrugge, J.W., van Cappellen, W.A., Hoeijmakers, J.H., and Grootegoed, J.A. (2004). The ubiquitin-conjugating DNA repair enzyme HR6A is a maternal factor essential for early embryonic development in mice. Mol. Cell. Biol. *24*, 5485–5495.

Sabens Liedhegner, E.A., Gao, X.H., and Mieyal, J.J. (2012). Mechanisms of altered redox regulation in neurodegenerative diseases—focus on S—glutathionylation. Antioxid. Redox Signal. *16*, 543–566.

Shalamanova, L., McArdle, F., Amara, A.B., Jackson, M.J., and Rustom, R. (2007). Albumin overload induces adaptive responses in human proximal tubular cells through oxidative stress but not via angiotensin II type 1 receptor. Am. J. Physiol. Renal Physiol. *292*, F1846–F1857.

Sheng, Z.H., and Cai, Q. (2012). Mitochondrial transport in neurons: impact on synaptic homeostasis and neurodegeneration. Nat. Rev. Neurosci. *13*, 77–93.

Stowers, R.S., Megeath, L.J., Górska-Andrzejak, J., Meinertzhagen, I.A., and Schwarz, T.L. (2002). Axonal transport of mitochondria to synapses depends on milton, a novel Drosophila protein. Neuron *36*, 1063–1077.

Tanabe, F., Yone, K., Kawabata, N., Sakakima, H., Matsuda, F., Ishidou, Y., Maeda, S., Abematsu, M., Komiya, S., and Setoguchi, T. (2011). Accumulation of p62 in degenerated spinal cord under chronic mechanical compression: functional analysis of p62 and autophagy in hypoxic neuronal cells. Autophagy *7*, 1462–1471.

Tanaka, K., Suzuki, T., Chiba, T., Shimura, H., Hattori, N., and Mizuno, Y. (2001). Parkin is linked to the ubiquitin pathway. J. Mol. Med. *79*, 482–494.

Tanaka, A., Cleland, M.M., Xu, S., Narendra, D.P., Suen, D.F., Karbowski, M., and Youle, R.J. (2010). Proteasome and p97 mediate mitophagy and degradation of mitofusins induced by Parkin. J. Cell Biol. *191*, 1367–1380.

Uytterhoeven, V., Kuenen, S., Kasprowicz, J., Miskiewicz, K., and Verstreken, P. (2011). Loss of skywalker reveals synaptic endosomes as sorting stations for synaptic vesicle proteins. Cell *145*, 117–132.

Van Humbeeck, C., Cornelissen, T., Hofkens, H., Mandemakers, W., Gevaert, K., De Strooper, B., and Vandenberghe, W. (2011). Parkin interacts with Ambra1 to induce mitophagy. J. Neurosci. *31*, 10249–10261.

Verstreken, P., Ly, C.V., Venken, K.J., Koh, T.W., Zhou, Y., and Bellen, H.J. (2005). Synaptic mitochondria are critical for mobilization of reserve pool vesicles at Drosophila neuromuscular junctions. Neuron *47*, 365–378.

Verstreken, P., Ohyama, T., and Bellen, H.J. (2008). FM 1-43 labeling of synaptic vesicle pools at the Drosophila neuromuscular junction. Methods Mol. Biol. *440*, 349–369.

Vives-Bauza, C., Zhou, C., Huang, Y., Cui, M., de Vries, R.L., Kim, J., May, J., Tocilescu, M.A., Liu, W., Ko, H.S., et al. (2010). PINK1-dependent recruitment of Parkin to mitochondria in mitophagy. Proc. Natl. Acad. Sci. USA *107*, 378–383.

Wirawan, E., Vanden Berghe, T., Lippens, S., Agostinis, P., and Vandenabeele, P. (2012). Autophagy: for better or for worse. Cell Res. *22*, 43–61.

Zenkel, M., Kruse, F.E., Naumann, G.O., and Schlötzer-Schrehardt, U. (2007). Impaired cytoprotective mechanisms in eyes with pseudoexfoliation syndrome/glaucoma. Invest. Ophthalmol. Vis. Sci. *48*, 5558–5566.

Ziviani, E., Tao, R.N., and Whitworth, A.J. (2010). Drosophila parkin requires PINK1 for mitochondrial translocation and ubiquitinates mitofusin. Proc. Natl. Acad. Sci. USA *107*, 5018–5023.